THE ASTROPHYSICAL JOURNAL, 418:804–811, 1993 December 1

HUBBLE SPACE TELESCOPE OBSERVATIONS OF PLANETARY NEBULAE IN THE MAGELLANIC CLOUDS. I. THE EXTREME TYPE I SMP 83/WS 35

MICHAEL A. DOPITA,[1] HOLLAND C. FORD,[2] RALPH BOHLIN,[2] IAN N. EVANS,[2] AND STEPHEN J. MEATHERINGHAM[1]

Received 1993 March 15; accepted 1993 May 17

ABSTRACT

We have obtained *Hubble Space Telescope* Planetary Camera images in both the Hα and the [O III] λ5007 emission lines of the planetary nebula SMP 83 alias WS35, alias N66 in the Large Magellanic Cloud. By combining these results with optical and UV spectrophotometry, absolute flux measurements, and dynamical and density information, we have been able to construct a fully self-consistent nebular model. This proves that SMP 83 is an extremely massive type I object having a central star having an effective temperature of 170,000 K and a luminosity of nearly $3 \times 10^4\ L_\odot$. The core mass is estimated in the range 1.0–1.2 $M_\odot$, for which the main-sequence mass was greater than $\sim 6\ M_\odot$. The nebular abundances are higher than the average for the LMC and show evidence for hot-bottom burning.

Subject headings: Magellanic Clouds — planetary nebulae: individual (SMP 83)

1. INTRODUCTION

The mass boundary between stars that evolve to Type I supernovae and those that evolve off the asymptotic giant branch (AGB) through the planetary nebular (PN) stage is still poorly determined. For this reason, the identification of planetary nebular nuclei (PNNs) that have evolved from the most luminous AGB stars is rather important. Such objects are rare, however, because the rate of evolution through the PN stage becomes much higher as the mass of the PNN increases, and the effect of this is to give a rather sharp cutoff in the luminosity function of PN corresponding to a core mass of about 0.7 $M_\odot$ in the Large Magellanic Cloud (LMC) (Dopita & Meatheringham (1991a, b). Indeed, the existence of such a cutoff in the luminosity function is the basis of the use of PN as standard candles (Ciardullo et al. 1989; Jacoby, Walker, & Ciardullo, 1990; Dopita, Jacoby, & Vassiliadis 1992).

In this paper we describe the results of imaging of a particular PN in the LMC, WS 35 in the catalog of Westerlund & Smith (1964), or SMP 83 in the catalog of Sanduleak, MacConnell, & Philip (1978). This PN was selected by the GTO team for observation with Planetary Camera (PC) of the *Hubble Space Telescope* (*HST*) on the basis of its extreme velocity of expansion and other characteristics, in particular its type I (nitrogen-rich; Peimbert 1978) nature strongly suggested that it may be a PN with a rather massive central star (Dopita, Ford, & Webster 1985). We have been able to combine the results of this imaging with the published optical and UV spectrophotometry to generate a self-consistent photoionization model. This allows us, for the first time, to place this object on the Hertzsprung-Russell diagram with reasonable accuracy and we have been able to prove that WS35/SMP 83 is indeed a PN whose central star has a mass close to the Chandrasekar limit.

[1] Mt. Stromlo and Siding Springs Observatories, Institute of Advanced Studies, The Australian National University, Private Bag, Weston Creek P.O., ACT 2611, Australia.

[2] Space Telescope Science Institute, Homewood Campus, Johns Hopkins University, Baltimore, MD 21218.

2. RESULTS OF *HST* IMAGING

2.1. *Observations and Data Processing*

The PN WS35/SMP 83 was observed with the Planetary Camera (PC) of *Hubble Space Telescope* (*HST*) on 1991 May 11 as part of the GTO program. Sequential exposures of 300 s were taken in the Hα line and in the [O III] λ5007 line. The filters employed were the F664N and the F502N, respectively. The wavelengths of the peak transmission and FWHM bandpasses of these filters are 5016, 30 Å and 6634, 132 Å, respectively. The PN was placed on the PC6 chip.

The STSDAS task CALWFPC was used to reprocess both images with the best available bias subtraction and flat-field correction available on 1992 May 5. In order to deconvolve the data, a 256 × 256 pixel subimage centered on WS35 was extracted and cleaned of cosmic-ray hits. A standard Lucy (1974) deconvolution was done using 50 and 100 iterations. Since the point-spread function (PSF) had not been explicitly determined by calibration observations with these filters, the PSF used in the deconvolutions was computed from the *HST* optical model in the code TINYTIM (Krist 1992). We found that, owing to the low signal levels of these observations, 100 iterations tended to amplify noise features and artifacts in the image. Part of this may be the result of the inadequacies of the PSF model.

2.2. *Results*

We show in Figure 1*a* the original F502N and F664N images of WS35 and in Figure 1*b* the images deconvolved using the Lucy algorithm. Inset on the Hα images we show the image of a star which is seen on the original frames at a radial distance of approximately 4.″9 from the nebula. This should therefore be quite a fair approximation to the point-spread function (PSF) at the time of the observation. The improvement in the PSF is quite apparent, and it is clear that the deconvolution procedure has produced no important artefacts in the PSF. All of the features seen in the deconvolved image can be seen in the original image, though at lower contrast because of smearing effects of the spherical aberration. There are two bright filaments, which we have labeled A and B in

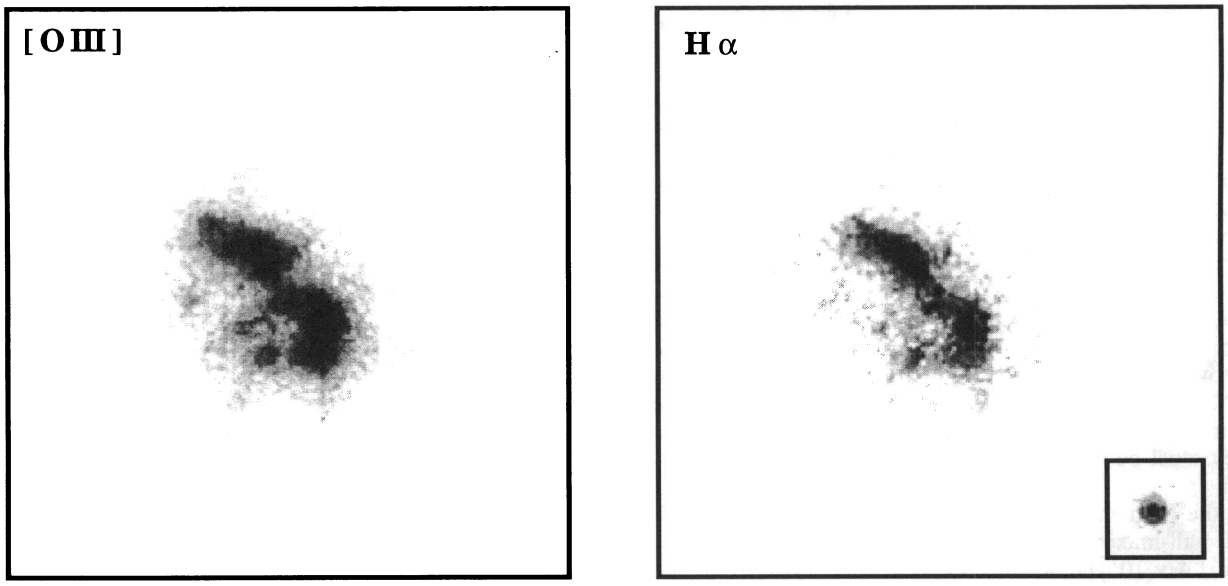

FIG. 1*a*

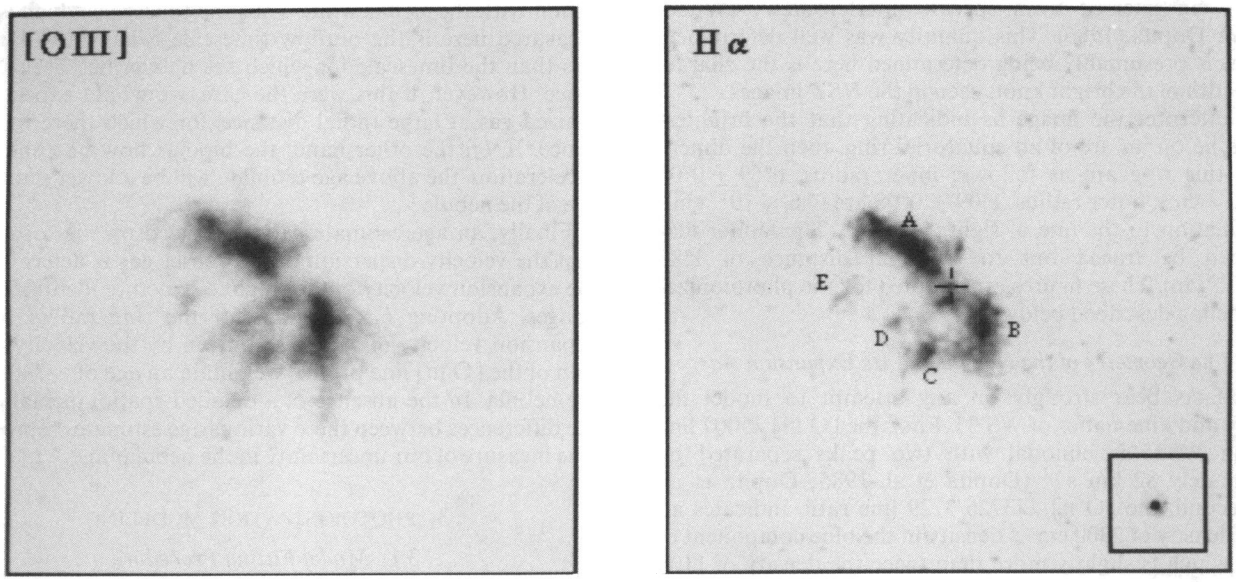

FIG. 1*b*

FIG. 1.—(*a*) The processed [O III] λ5507 and Hα PC images of SMP 83 (alias WS 35, alias N66). Each image is 5.5 arcsec^2. The inset is the Hα image of a star 4".8 away and gives a good idea of the PSF at this wavelength. North is in PA 45°, and east is to the right in this figure. (*b*) As (*a*), but after deconvolution through the Lucy (1974) algorithm. Note the improvement in the PSF. The principal filaments refered to in the text are marked, as is the position of the exciting star.

Figure 1*b*, and three fainter filaments labelled C, D, and E. All of the structures seen in Figure 1 can also be seen in the somewhat deeper [O III] λ5007 Faint Object Camera image of WS35 published by Blades et al. (1992). However, this image emphasises the fainter filamentary extensions to the image which are weakly visible in our [O III] image. These features are relatively stronger in the [O III] image, suggesting that this material is optically thin to the ionising radiation.

The Blades et al. images also allow us to unambiguously identify the exciting star, identified by a cross in Figure 1*b*. The fact that this is also detected in our Hα image allows us to measure the flux of this star by reference with the (known) Hα flux of the nebula. Using the filter transmission curve given in the WF/PC Instrument Handbook, we find that 61.2% of the observed nebular flux is due to Hα, the rest being [N II] emission. From the ratio of observed counts, we measure a stellar flux of $2.07 \pm 0.8 \times 10^{-17}$ ergs cm^{-2} s^{-1} Å^{-1} at Hα. This will be used (below) to determine the luminosity of the star directly.

Approximately 45% of the total observed [O III] λ5007 flux is produced by the two brightest filaments. The overall bipolar "butterfly" appearance of the nebula is similar to galactic PNs such as those illustrated in Balick's (1989) paper as examples of "late-type" "ellipticals" or "butterflies." It is also similar to type I PNs in our own Galaxy such as NGC 6302 or NGC 6537. In particular, the structure of the nebula is very like the short-exposure image of He 2-111 (Webster 1978) and is

remarkably reminiscent of the *HST* image of NGC 2440 (Heap 1992), down to the two bright arcs, and the position of the exciting star with respect to these.

The morphology suggests that the nebula may consist of a partially equatorial ring and a bipolar extension. However, if WS 35/SMP 83 had the large faint lobes observed in He 2-111 or in NGC 2440, then it is highly unlikely that these would be detectable in our images, thanks to their low emissivity relative to the core. The existence of faint, radially directed streamers visible in the images suggests such giant lobes may exist. However, since they would extend over several arcseconds, they should be readily observable in images taken with a ground-based telescope. The [O III] images of Jacoby et al. (1990) show no such extension, and the measured size of the nebula, 1".3, corresponds fairly well to the total extent of the faint filaments seen in the *HST* images. Thus, if giant lobes exist, they must be of very low emissivity, and therefore optically thin.

All of the filaments are resolved with a characteristic full width at half-maximum of approximately 0".2. This corresponds to 1.4×10^{17} cm at the 49 kpc we have assumed as the distance of the LMC (Feast & Walker 1987; Feast 1988). This can be compared with the characteristic dimension of 2.4×10^{17} cm inferred from speckle interferometry (Wood, Bessell, & Dopita, 1986). This quantity was well determined, and what is presumably being determined here is the characteristic width of the bright knots seen in the *HST* images.

If we interpret the image as indicating that the brightest filaments lie on an arc of an equatorial ring, then the dimensions of this ring are as follows: inner radius, $0''.69 \pm 0''.08$ (4.8×10^{17} cm); outer radius, $1''.09 \pm 0''.08$ are (7.6×10^{17} cm); and inclination to the line of sight, $63° \pm 5°$. The fainter filaments can be traced out to a radial distance of 1".86 (1.3×10^{18} cm). These figures are adopted for the photoionization modeling described below.

2.3. *The Geometry of the Nebula and Its Expansion Age*

Three facts bear strongly on any attempt to model the geometry and kinematics of WS 35. First, the [O III] λ5007 line profile in WS35 is bimodal with two peaks separated by approximately 82 km s^{-1} (Dopita et al. 1985; Dopita et al. 1988). Second, the [O II] $\lambda\lambda$3726/3729 line ratio indicates an electron density of 2300 cm^{-3} density in the blue component of the line, which is slightly more than twice the density of 1100 cm^{-3} determined for the red component. Third, the mean velocity of the blue component, 232.5 km s^{-1}, is most likely the systemic velocity of the planetary, since this velocity is only 13.5 km s^{-1} greater than the systemic velocity at this position predicted by the rotation curve solution for the LMC presented by Meatheringham et al. (1988a) when we separate LMC PNs into two age groups according to their estimated core mass, we find that the young PNs like WS35 have a velocity dispersion of 15 km s^{-1} relative to this solution, consistent with that determined using the blue component of WS35. If, on the other hand, we had taken the systemic velocity of WS35 as the mean of the two components (278 km s^{-1}), then its systemic velocity would differ by some 59 km s^{-1} from rotation curve solution. Such a large value is very unlikely for a PNN having a relatively massive and short-lived progenitor. Finally, we note that the line profile shows that there is very little [O III] emission at this systemic velocity of the nebula.

If we make the physically plausible assumption that the high surface brightness filaments A and B are the high-density gas, then the remaining low surface brightness filaments are low-density, redshifted gas. This interpretation would then be fairly consistent with the fraction of the total emission seen in the filaments A and B. From the images, these give 45% of the total [O III] emission, whereas from the low-velocity part of the [O III] line profile accounts for 54% of the total emission. In this model filaments A and B represent optically thick material associated with a reservoir of unionized material near the equatorial plane, and the fainter filaments are part of an optically thin, high-velocity, one-sided polar flow.

A crude expansion age can be derived by dividing a characteristic size of the nebula by its expansion velocity. The filaments in our highly resolved image have a characteristic radial extent of approximately 1".5. If viewed through an angle θ relative to the plane of the sky, the expansion age will then be approximately $\tau = (r/V_{\rm exp}) \tan \theta$. Adopting a radius of 10^{18} cm from the images, an expansion velocity of 82 km s^{-1} from the line profiles and $\tan \theta \sim 0.6$ estimated from the ring parameters given above, we have $\tau \sim 2400$ yr. This age estimate is capable of more subtle interpretation. If the reservoir of unionized material is massive and slow moving, then the velocity of expansion which is measured is the velocity of outflow of ionized gas from the ionization fronts, accelerated by its interaction with the stellar wind. Thus the timescale which is being measured here is the outflow timescale, which may be much less than the timescale for which the nebula has been in existence. However, if this were the case, we would expect to see ionized gas at large radial distance, for which there is no evidence. If, on the other hand, the bipolar flow has undergone acceleration, the above age estimate will be a lower limit to the age of the nebula.

Finally, an age estimate can be derived on the assumption that the velocity dispersion of the denser gas is determined by the expansion velocity of the ringlike structure identified in the images. Adopting 6×10^{17} cm for the ring radius, and an expansion velocity of 57 km s^{-1} given by the velocity dispersion of the [O III] line profile, we obtain an age of $\sim$3400 yr for the nebula. In the absence of a detailed spatiokinematic map, the differences between these various age estimates represents a true measure of our uncertainty in the nebular age.

3. PHOTOIONIZATION MODELING

3.1. *Model Fitting Procedure*

A high-quality global optical spectrum of SMP 83/WS 35 has been presented by Meatheringham & Dopita (1991a). This demonstrates that this object belongs to Peimbert's (1978) type I class, showing both high excitation and strong emission lines of nitrogen. We reproduce the observed spectrum in Table 2 to facilitate comparison with the models. An attempt was made by Dopita & Meatheringham (1991a, b) to model this and other type I PNs using the modeling code MAPPINGS 1 (Binette, Dopita, & Tuohy 1985) to compute spherically symmetric, isobaric nebulae excited by a central star having a blackbody spectral distribution. In general, the models for type I planetary nebulae show similar problems, as pointed out by Dopita & Meatheringham (1991a, b). In summary, these are as follows. First, the low-excitation lines are predicted to be stronger than observed. Second, the [O III] and [S III] electron temperatures are predicted too low (although electron temperatures defined through the use of species with lower excitation potential such as N II or O II are in good agreement with observation). Third, the models frequently strongly underesti-

mate the line intensities of high-ionization species such as [Ne v]. For the purposes of comparison, the specific parameters of the model given in Dopita & Meatheringham (1991a) are as follows. Central star luminosity and temperature; $L/L_{\odot} = 2880$; $T_{\rm eff} = 170{,}000$ K, nebular density $N(\rm H) = 2880$ cm^{-3} (at 10,000 K, isobaric model), inner nebular radius $r_{\rm in} = 5 \times 10^{16}$ cm and outer nebular radius, $r_{\rm out} = 3.8 \times 10^{17}$ cm. Clearly these sizes are inconsistent with the results of the nebular imaging.

When we consider the UV lines (Meatheringham et al. 1993) the comparison becomes even worse. Virtually all of the UV resonance and intercombination lines are predicted too weak by the simple photoionization model. These lines are mainly produced in the inner part of the nebula where the ionization parameter, Q, is high, requiring either a high stellar luminosity, or else a low nebular density. In the single-zone model, neither of these parameters can be attained, since the nebular luminosity is in this case coupled to the stellar luminosity, and the inner nebular radius is about as small as it can be in the model.

The solution to these problems is evident from the *HST* images. It is clear that a multizone photoionization model must be used to adequately represent the equatorial ring and its bipolar extensions. The simplest model is one of an optically thick ring with optically thin extensions such has been used with success by Clegg et al. (1987) to model NGC 3918. In the case of WS 35/SMP 83, this type of model should be adequate.

For the photoionization modeling presented here, we have used the improved photoionization/shock modeling code MAPPINGS 2 (Sutherland & Dopita 1993). Among the improvements relevant to this exercise, it includes all important ionization stages up to fully stripped Fe and Ni, has a much improved adaptive spatial gridding procedure, explicitly computes all nebular continua, and operates with a much extended and improved set of atomic parameters, particularly with respect to the resonance and intercombination lines.

We adopt a photoionization model (see Fig. 2) in which the global spectrum is the weighted mean of an optically thick component and an optically thin component of arbitrary optical depth; $F_{\rm tot} = \omega F_{\tau(\rm H)\to\infty} + (1 - \omega)F_{\tau(\rm H)=\tau_0}$. The optically thick component is assumed to be isobaric and characterized by the pressure which reproduces the observed [O II] 3726/3729 Å line ratio for this component, $P/10^4$ K $= 3600$ cm^{-3}. This density also agrees well with that given by the observed [S II] $\lambda\lambda$6731/6717 line ratio. The nebula is assumed to have an inner radius of 4.5×10^{17} cm, the measured size. The optically thin component is taken to be isochroric with a density of 1000 cm^{-3}, given by the observed [O II] $\lambda\lambda$3726/3729 line ratio for this component. Since the optically thin gas is presumed to have its origin at the ionisation fronts of the dense material, it is assumed to have the same inner radius, 4.5×10^{17} cm. In a fully self-consistent model, the outer radii of the two components should also agree with what is indicated by the imaging. Apart from the abundances of the elements, the free parameters of the model are the flux-weighting factor ω, the optical depth of the optically thin component, the effective stellar temperature, $T_{\rm eff}$, and the ionization parameter $Q(\rm H)$. Thus, even within the context of such a simple model, the exercise of model fitting is by no means trivial.

Of these parameters, $Q(\rm H)$ and $T_{\rm eff}$ are particularly well constrained. A decrease in $Q(\rm H)$ produces a dramatic decrease in the relative strength of the high-ionization lines arising in the optically thin zone, particularly in the UV. In order to obtain strong enough high-excitation lines, we require $Q \geq 1.2 \times 10^8$ cm s^{-1} for this component. On the other hand, the physical thickness of the optically thick component varies directly as the ionization parameter, since this determines the Strömgren column. Models which produce the correct inner and outer radii in the optically thick component (4.5×10^{17} and 6.3×10^{17} cm, respectively) require a mean ionization parameter of about 10^8 cm s^{-1}.

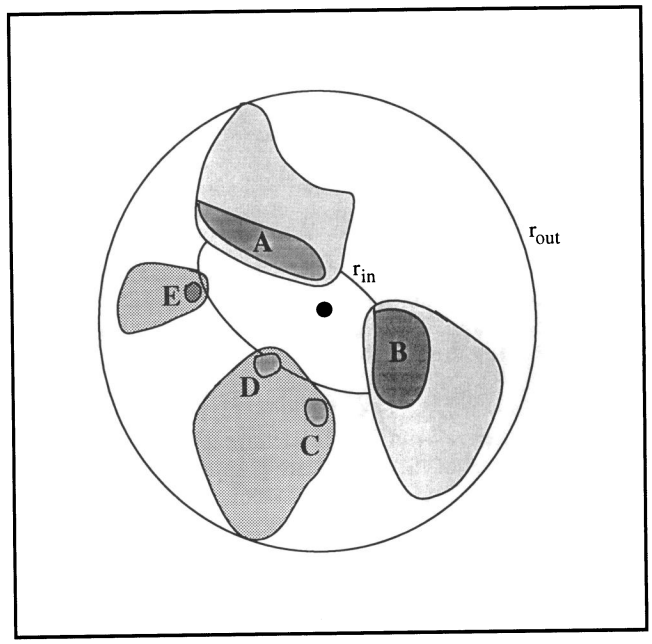

FIG. 2.—The idealized model used in the photoionization modeling. It is assumed that the filaments A to E (*shaded dark*) lie in a dense equatorial ring of radius $r_{\rm in}$ and that these are optically thick to the UV radiation. The ionized flow streaming from the ionization fronts in this ring forms a filamentary, optically thin region of lower density (*shaded light*). The dense component has ~6% covering factor, and the optically thin material a ~30% covering factor with respect to the central star.

The effective stellar temperature $T_{\rm eff}$ is constrained fundamentally by the ionization state of helium, and by the He II lines in particular, since the strength of these lines is effectively independent of the ionization parameter over the region of interest. However, the strength of these lines is dependent on the optical thickness of the nebula, since low optical depth leads to an enhancement of He II lines and a suppression of the He I lines. However, making the extreme assumption that the optically thin zone has negligible optical depth and assuming that the relative contributions of the optically thick and thin zones are equal (so as to be in accord with the imaging and the high-resolution spectrophotometry), we can obtain a lower bound on the temperature. An upper bound can be obtained by the (clearly incorrect) assumption that the nebula is entirely optically thick. These estimates constrain the temperature to lie in the narrow range 150,000 K $< T_{\rm eff} <$ 175,000 K.

Our modeling procedure is therefore to take $T_{\rm eff}$ as a free parameter within the limits given above, and choose the Q which gives the correct outer radius for the optically thick component in an isobaric model having the correct mean [O II] $\lambda\lambda$3726/3729 line ratio. We then construct the (isochoric) optically thin model which corresponds to these parameters, allowing for the lower density in this component. The optical depth is chosen so as to give an outer radius which agrees with total extent of the ionized material in the images (1.3×10^{18} cm). We then seek linear sums of the optically thin and opti-

cally thick models which produce as nearly as possible a constant ratio of observed to predicted line intensities over the full range of ionization states of a given element. If the abundance of an individual element is incorrect, then this will appear as an (approximately constant) offset in the ratio of observed-to-predicted line intensity over the whole range of ionization stages. The abundance can then be altered in a subsequent run so as to bring these ratios for that element to close to unity.

Within the constraints and assumptions of the two-component model itself, this procedure produces a fully self-consistent result, in that it agrees with the observed density and the physical size of the two components, and also gives the correct global line strengths and excitation state of the nebula.

3.2. *Results*

The parameters of our final model are given in Table 1, and the line intensities of this model are compared with the observations in Table 2. Here model M060 is the optically thin component, and M061, the optically thick component. The relative weighting factor ω, defined above, is found to lie between 0.6 and 0.4. This range encompasses the values determined above from the imaging and the [O II] and [O III] line profiles: 0.45 and 0.54, respectively. We adopt $\omega = 0.5$, close to the mean of these other estimates, and which gives the best-fit solution to the line spectrum. The weighted average spectrum which results is shown in the "Sum" column and is to be compared with the observed line fluxes of the final column of Table 2. Figure 3 shows the relative contributions of the optically thin and optically thick components to this best-fit solution for all the lines used in the fitting procedure. For this, we have used neither line blends nor the fainter of two lines with known intensity ratio such as the [O III] λ4959 or the [N II] λ6548 lines. This figure emphasises the need for both optically thin and optically thick components to achieve a satisfactory fit to the observations. In Figure 4 we plot the observed and the theoretical line intensities for each element over all observed ionization stages. As can be seen, the scatter is sufficiently small to give confidence that the elemental abundances have been determined to within $\pm 15\%$. Paradoxically, the worst fit is for the He lines, since we had to take the effective temperature near the upper limit of what is allowed by the

TABLE 1

MODEL PARAMETERS FOR SMP 83

A. INFERRED STELLAR PARAMETERS

Parameter	Value
$L/L_\odot$	27,000 ± 6000 (from nebular model) 32,000 ± 12,000 (from Hα image)
$M/M_\odot$	0.98 ± 0.17 (H-burning); ~1.2 (He-burning)
$T_{\rm eff}$	170,000 ± 10,000 K

B. ABUNDANCES OF THE ELEMENTS BY NUMBER WITH RESPECT TO H [error ~ 10%])

He	C	N	O	Ne	S	Ar
0.13	2.6E−5	1.15E−4	4.17E−4	5.10E−5	2.40E−5	2.80E−6

C. PROPERTIES OF NEBULAR COMPONENTS

Parameter	Value
Optically Thin Component:	
N(H)	1000 cm^{-3} (isochoric)
$r_{\rm in}$	4.5E17 cm
$r_{\rm out}$	7.5E17 cm
τ(H)$_{\rm final}$	1.94
$M_{\rm neb}$	0.4 $M_\odot$
Optically Thick Component:	
N(H)	3600 cm^{-3} (at 10,000 K; isobaric)
$r_{\rm in}$	4.5E17 cm
$r_{\rm out}$	7.0E17 cm
$M_{\rm neb}$	0.19 $M_\odot$

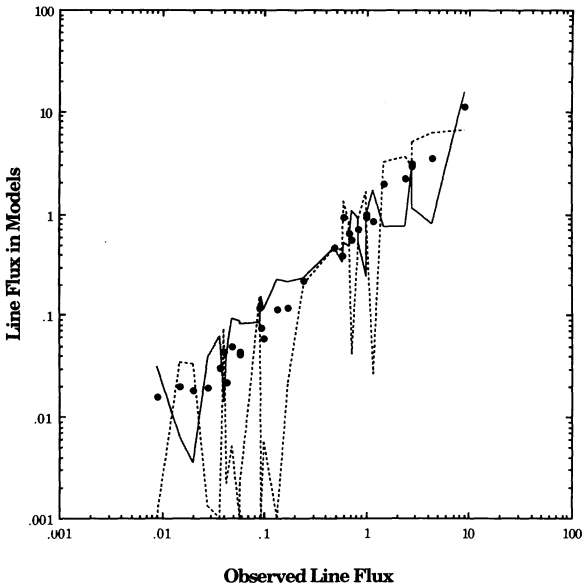

FIG. 3.—The emission-line flux predicted in the models is plotted against the observed line flux with respect to Hβ = 1.0 for all lines that are unblended, or which represent the brighter component of a doublet with known intensity ratio. The contribution of the optically thick component in the models is represented by a solid line, and that of the optically thin component by a dotted line. The weighted sum of these is represented by dots. Note how the two components complement each other in the global fit.

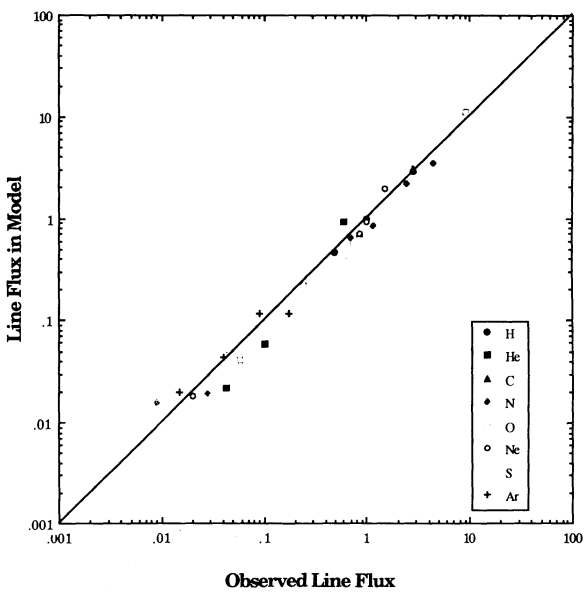

FIG. 4.—As Fig. 3, except that lines of each element are distinguished. It is clear that the accuracy of the fit approaches that of the observations, and that the elemental abundances have been determined to an accuracy of order 15%.

TABLE 2

OBSERVED AND MODELED LINE INTENSITIES WITH RESPECT TO Hβ = 100.0[a]

Ion	Wavelength (Å)	M0060	M0061	Sum	Observed
H I	4100	25.72	25.93	25.82	26.30
	4340	46.81	46.94	46.88	48.60
	4861	100.00	100.00	100.00	100.00
	6563	289.6	285.1	287.3	278.2
He I	4472	0.22	4.19	2.20	4.30
	5876	0.57	11.38	5.97	10.00
	6678	0.16	3.25	1.71	3.20
He II	4686	134.0	52.20	93.10	60.10
C III]	1909	91.44	52.10	71.77	85.00
C IV	1549	502.0	115.02	308.5	280.0
[N I]	5200	0.10	3.12	1.56	0.90
[N II]	5755	0.13	3.82	1.98	2.80
	6584	2.59	168.2	85.39	115.3
N III]	1750	81.34	48.79	65.07	68.00
N IV]	1487	363.2	75.78	219.5	243.0
N V	1245	616.3	80.94	348.6	444.0
[O I]	6300	0.10	8.73	4.37	5.70
[O II]	7325	0.21	8.09	4.15	5.80
	3727	4.08	106.6	55.34	73.20
O III	1666	43.71	33.55	38.63	59.00
[O III]	4363	20.10	23.76	21.93	24.30
	4959	225.1	546.5	385.8	313.3
	5007	648.4	1574.0	1111.2	896.0
[Ne III]	3868	50.14	90.66	70.40	84.90
[Ne IV]	2426	318.50	74.82	196.7	149.7
	4725	3.30	0.35	1.83	2.00
[Ne V]	3346	59.91	8.75	34.33	26.1
	3426	163.00	23.82	93.41	99.20
[S II]	4069.76	0.10	6.19	3.10	3.70
	6717	0.10	15.20	7.60	9.50
	6731	0.10	22.62	11.31	13.30
[S III]	6312	0.53	9.34	4.93	4.90
[Ar III]	7136	2.18	21.36	11.77	17.2
[Ar IV]	4740	14.94	8.55	11.74	9.00
[Ar V]	6435	3.40	0.65	2.03	1.50
[Ar V]	7006	7.30	1.39	4.34	4.00

[a] Arranged by element and ionization stage for unblended lines.

helium excitation in order to correctly reproduce the (high)-excitation state of the other elements. This is presumably the result of our assumption of a blackbody photon distribution for the central star. In reality, blanketing by heavier elements will tend to reduce the number of hard photons at a given effective temperature (Gabler, Kudritski, & Mendez 1991).

The flux of the central star is determined primarily by the density and the observed physical thickness of the optically thick component, since this is a direct measure of the Strömgren column. However, a more indirect estimate can be obtained from the observed Hβ flux. For SMP 83, the observed absolute Hβ flux, corrected for atmospheric absorption and interstellar reddening, is $\log F(\mathrm{H}\beta) = 34.90$ ergs s^{-1} (Meatheringham, Dopita, & Morgan 1988b). From the images, each bright arc is $\sim 0''.2$ wide and $\sim 0''.8$ long (1.4×10^{17} cm $\times$ 5.5×10^{17} cm). Thus the two of them subtend a solid angle not in excess of ~ 0.76 sr, or 6% of the solid angle, as seen from the central star. Thus, from the models, the optically thick component should have a luminosity of $\log F(\mathrm{H}\beta) = 34.18 + \log (L/10^4\ L_\odot)$ ergs s^{-1}. Since we require that this component account for half the total flux to fit the relative line intensities, we have $L \sim 2.6 \times 10^4\ L_\odot$, in good agreement with the value derived from the Strömgren column. For the optically thin material we can then infer an angular covering fraction of ~ 0.33. These figures provide the basis of the nebular mass estimates of Table 1. The sum of the nebular masses of the two components ($0.59\ M_\odot$) is similar to the mass estimate determined from the one-zone model, since both depend on the measured Hβ flux, but of course, our estimated luminosity of the central star is much higher, as a result of leakage of UV photons out of the nebula.

Provided that we can take the temperature of the central star to be given by the photoionization model, the observed flux of the central star, $2.07 \pm 0.8 \times 10^{-17}$ ergs $\mathrm{cm}^{-2}\ \mathrm{s}^{-1}\ \text{Å}^{-1}$ at Hα, can be used to directly determine the luminosity of the central star. From this we find $L/L_\odot = 32{,}000 \pm 12{,}000\ L_\odot$, in excellent agreement with that given by the model. We can therefore have considerable confidence that the position of the star on the H-R diagram has been reliably determined.

4. DISCUSSION

From the models presented in Tables 1 and 2, it is clear that the compound photoionization model removes the problems of the simple model as a result of the contribution of the high-

temperature optically thin component. The leakage of the stellar UV radiation from the nebula has a dramatic effect on our estimate of stellar luminosity, which increases by over an order of magnitude, from 2880 $L_\odot$ to somewhere in the range 1.9×10^4 to 3.5×10^4 $L_\odot$. Coincidentally, this estimate is much closer to that given by Dopita et al. (1985), although this was based on a spurious estimate of the Zanstra temperature. Whether the central star is hydrogen- or helium-burning, it is clear that it has a massive central star, which may even be approaching the Chandrasekar limit. The extreme position of this PN on the Hertzsprung-Russell diagram is made clear in Figure 5, in which we have also plotted the positions of all the other PNs placed on the H-R diagram by Dopita & Meatheringham (1991a, b).

The luminosity of the PNN depends upon whether it is on a H-burning or He-burning track, which in turn depends on the phase of the thermal pulse at which the transition to PN occurs. Dopita et al. (1992) argue that the distribution of the LMC PNNs on the Hertzsprung-Russell diagram strongly argues in favor of the hypothesis that the majority of these are helium-burners. For the hydrogen-burning objects, the core mass is well determined, since the evolution to high temperature occurs at an almost constant luminosity, L, which may be expressed in terms of the core mass (Wood & Zarro 1981; Dopita et al. 1992);

$$(L/L_\odot) = 57340[(M_c/M_\odot) - 0.507] \quad (4.1)$$

from which we can derive the core mass given in Table 2,

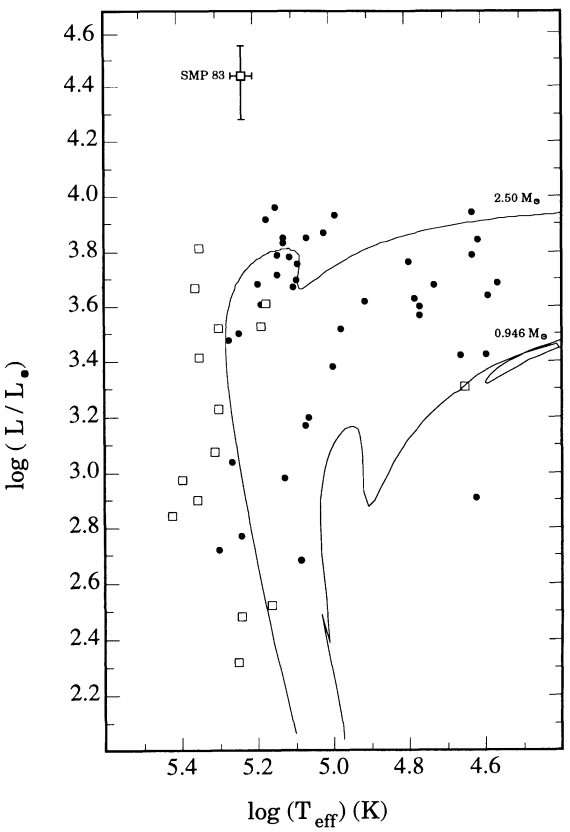

FIG. 5.—The H-R diagram for the PNs in the LMC (from Dopita & Meatheringham 1991b). Here type I PNs are shown as open squares. This clearly demonstrates the extremely luminous nature of SMP 83.

$M_c = 0.98 \pm 0.17$ $M_\odot$. If helium-burning, the core mass is somewhat more uncertain, since the luminosity is much more variable and sometimes multivalued as a function of temperature. However, at the high effective temperature observed, it should be fairly well determined and of order 1.2 $M_\odot$. Dopita et al. (1992) give the relation between the core mass M_c during the PN phase of evolution and the abundance and mass on the main sequence, M:

$$(M_c/M_\odot) = 0.493(Z/Z_\odot)^{-0.035}[1 + 0.147(M/M_\odot)] . \quad (4.2)$$

This relation is sensitive to the treatment of mass loss on the asymptotic giant branch. From equation (4.2) we find $M = 6.4$ $M_\odot$ (if hydrogen-burning) and ~ 9 $M_\odot$ (if helium-burning). A lower mass limit for the precursor star can be obtained by simply co-adding the core mass and the mass of the ionized material. This gives $M \geq 1.6$ $M_\odot$ if the PNN is hydrogen-burning or $M \geq 1.8$ $M_\odot$ if helium-burning.

Given the high core mass, the rather long dynamic age (2500–3500 yr) inferred above presents somewhat of a problem. According to PNN evolutionary models (Wood & Faulkner 1986; Vassiliadis 1992), the evolution of hydrogen-burning central stars of this mass is exceedingly rapid. Indeed, such a star will remain luminous for only ~ 100 yr from the time that it becomes hot enough to start to ionize its nebula. The central star has an ionizing photon production rate of 1.4×10^{48} s^{-1}, so that it is capable of driving an ionization front into the cloud material at an initial velocity of ~ 1000 km s^{-2}. Therefore, the *minimum* ionization timescale, the time taken to ionize the dense material at the current stellar luminosity, is 100 yr and may be considerably longer than this, since the flow from the clouds is observed to be optically thick. If we wish to preserve the hypothesis that the central star is hydrogen-burning, we must therefore conclude that the cloud material has been ionized in situ, since it would have had no time to expand in the time available. If this were the case, then the cloud material would have to be identified with envelope material ejected during the last helium shell flash episode, $\sim 20{,}000$ yr ago, based on the observed radius, and an assumed outflow velocity of 10 km s^{-1}. If, on the other hand, the central star is helium burning, these problems are alleviated, since the central star evolves much more slowly and remains luminous for in excess of 1000 yr. Given the very short evolutionary timescales associated with the hydrogen-burning stars, we would expect to be able to see evolution of the central star within the lifetime of the *HST*, or detect such evolution over a few years from evolution in the spectral character of the PN.

The combination of the UV and optical spectra has permitted us for the first time to obtain a reliable set of abundances. The effect of the addition of an optically thin region has been generally to increase our earlier (Dopita & Meatheringham 1991a, b) estimates of the abundances. For the more massive α-process elements, Ne, Ar, and S, which ought not to be influenced by dredge-up processes in the central star, we find a basal metallicity 0.27 dex higher than the mean of the LMC H II regions and SNRs found by Russell & Dopita (1990, 1992). This is exactly consistent with the observed enhancement in the O abundance relative to the corresponding mean LMC value for the H II regions. Although we can draw no firm conclusions from a single object, this is nonetheless an indication that the apparent decrease in the O abundance found by Dopita & Meatheringham (1991b) may be an artifact of the modeling procedure, and not a result of O-N processing, as they suggested.

The elements He and N both show the enhancements expected in a type I object. In particular, the N abundance is much more reliably established, since all the principal stages of ionization are observable. The N/O abundance ratio of 0.28 is at the lower limit of what has been found for the type I PNs in the Magellanic Clouds which may suggest that the degree of N dredge-up may finally decrease for the most massive stars.

The low C abundance, assumed to pertain in type I PNs has been confirmed. However, this cannot be taken as concrete evidence dredge-up in the ejected envelope material. The C + N abundance is very similar to that which would be expected on the basis of the O, Ne, S, and Ar abundances. Thus, the observed C and N abundances are consistent with CN processing in the material that was already there, but little or no dredge-up of CN processed material is allowed. This suggests that "hot-bottom burning" (Kaler 1985) rather than dredge-up has determined the observed abundances of C and N in this planetary.

5. CONCLUSIONS

In this paper, thanks to images made by the *HST*, we have been able to produce the first fully self-consistent model for a Magellanic Cloud planetary nebula. This has proved that WS 35/N66/SMP 83 is the most luminous PN so far identified in the LMC. With a core mass of between 1.0 and 1.2 $M_{\odot}$, it is clearly derived from a main-sequence star which is near the upper mass limit of those which can finally evolve to white dwarfs. Indeed, in both the Magellanic Clouds, it is only surpassed by the nucleus of the type I PN N67 (SMP 22) in the SMC. This has been detected through the thermal emission of the central star at X-ray wavelengths, placing it at log $(L/L_{\odot}) = 4.6 \pm 0.7$; log $(T_{\rm eff}) \sim 5.5$ (Wang 1991).

The dynamical age we derive appears to be inconsistent with the age estimated on the hypothesis that the central star left the AGB as a hydrogen-burning star, suggesting that it may well be a helium burner.

The abundances we derive for the nebula show clear evidence for "hot-bottom burning" of C to N, but little evidence of dredge-up of CN processed material on the asymptotic giant branch and no evidence for ON processing hypothesised by Dopita & Meatheringham (1991b).

The results described in this paper are based on observations with the NASA/ESA *Hubble Space Telescope*, obtained at the Space Telescope Science Institute, which is operated by the Association of Universities for Research in Astronomy, Inc., under NASA contract NAS5-26555. We wish to acknowledge support through NASA grant NAG5-1630, and support through the International Science and Technology Section of the Australian Department of Industry Technology and Commerce. We thank D. J. Lindler who set up the procedure for reprocessing the data and provided the deconvolved images.

The Imaj software used to generate the final images published in this work are part of the "Scientific Data Handling Suite" software developed by (Ralph S. Sutherland) at MSSSO, with the support of a grant from the Australian Apple University Development Fund in 1992.

REFERENCES

Balick, B. 1989, in IAU Symp. 131, Planetary Nebulae, ed. S. Torres-Peimbert (Dordrecht: Kluwer), 83
Binette, L., Dopita, M. A., & Tuohy, I. R. 1985, ApJ, 297, 476
Blades, J. C., et al. 1992, ApJ, 398, L41
Ciardullo, R., Jacoby, G. H., Ford, H. C., & Neill, J. D. 1989, ApJ, 339, 53
Clegg, R. E. S., Harrington, J. B., Barlow, M. J., & Walsh, J. R. 1987, ApJS, 314, 551
Dopita, M. A., Ford, H. C., & Webster, B. L. 1985, ApJ, 297, 593
Dopita, M. A., Jacoby, G. H., & Vassiliadis, E. 1992, ApJ, 389, 27
Dopita, M. A., & Meatheringham, S. J. 1991, ApJ, 367, 115
———. 1991b, ApJ, 377, 480
Dopita, M. A., Meatheringham, S. J., Webster, B. L., & Ford, H. C. 1988, ApJ, 327, 639
Feast, M. W. 1988, in The Extragalactic Distance Scale, ed. S. van den Bergh & C. J. Pritchet (ASP Conf. Ser. 4), 9
Feast, M. W., & Walker, A. R. 1987, ARA&A, 25, 345
Gabler, R., Kudritski, R. P., & Mendez, R. 1991, in Stellar Atmospheres: Beyond Classical Models, ed. L. Crivellari, I. Hubeni, & D. G. Hummer (NATO ASI Series), 143
Heap, S. 1992, HST Photo Release, STSCI-PRC92-12
Jacoby, G. H., Walker, A. R., & Ciardullo, R. 1990, ApJ, 365, 471
Kaler, J. B. 1985, ARA&A, 23, 89
Lucy, L. B. 1974, AJ, 79, 745
Meatheringham, S. J., Aller, L. H., Keyes, C. D., Stecher, T. P., Maran, S. P., Michalitsianos, A. G., & Gull, T. R. 1993, in preparation
Meatheringham, S. J., & Dopita, M. A. 1991a, ApJS, 75, 407
———. 1991b, ApJS, 76, 1085
Meatheringham, S. J., Dopita, M. A., Ford, H. C., & Webster, B. L. 1988a, ApJ, 327, 651
Meatheringham, S. J., Dopita, M. A., & Morgan, D. H. 1988b, ApJ, 329, 166
Peimbert, M. 1978, in IAU Symp. 76, Planetary Nebulae, ed. Y. Terzian (Dordrecht: Reidel), 215
Russell, S. C., & Dopita, M. A. 1990, ApJS, 74, 93
———. 1992, ApJ, 383, 508
Sanduleak, N., MacConnell, D. J., & Philip, A. G. D. 1978, PASP, 90, 621 (SMP)
Sutherland, R. S., & Dopita, M. A. 1993, ApJS, 88, 253
Vassiliadis, E. 1992, PhD thesis, The Australian National University: Canberra
Wang, Qingde. 1991, MNRAS, 252, 47P
Webster, B. L. 1978, MNRAS, 185, 45P
Westerlund, B. E., & Smith, L. F. 1964, MNRAS, 127, 449
Wood, P. R., Bessell, M. S., & Dopita, M. A. 1986, ApJ, 311, 632
Wood, P. R., & Faulkner, D. J. 1986, ApJ, 307, 659
Wood, P. R., & Zarro, D. M. 1981, ApJ, 247, 247